JOURNAL OF MATERIALS SCIENCE 29 (1994) 6033–6040

Interface contribution to the SiC–titanium and SiC–aluminium tensile strength prediction

Part I *Interface characterization by fragmentation tests*

L. MOLLIEX*, J-P. FAVRE‡, A. VASSEL, M. RABINOVITCH
Materials Science Department, ONERA, Châtillon, F-92320, France

Fragmentation tests of single SiC filaments embedded in an aluminium (1050 and 5083 alloys) or a titanium (Ti–6Al–4V) matrix have been analysed in an effort to obtain the interface contribution in terms that could be incorporated into a tensile fracture model for unidirectional composites. Depending on the matrix, two regimes of interfacial stress transfer can be distinguished within the whole range of tested temperatures. For the SCS2/5083 system, plastic deformation of the alloy limits the stress transfer, and the interface contribution thus finds its expression in the shear stress of the matrix. for the SCS6/Ti–6Al–4V system, friction is the leading process and the interface contribution strongly depends on the stress state around the fibre. Assuming a temperature dependent compressive radial stress up to 925 °C, an effective transfer shear stress may be easily calculated for unidirectional SCS6/Ti–6Al–4V composites.

1. Introduction

Fragmentation testing of monofilament model composites is now well established as a very convenient means for analysing the basic response of fibre–resin interfaces. Due to the difficulty of specimen preparation, the method has been applied less frequently to metal matrix systems [1–5]. In the present paper, complete results on SiC–titanium and SiC–aluminium monofilament model composites, partly reported recently [6–9], are presented in parallel. The objective is two-fold

(i) to characterize the interfacial mechanical response in relation to fibre and metallic matrix properties as a result of the manufacturing process or protective coating efficiency, and

(ii) to introduce mechanical information about fibre–matrix stress transfer into a simplified tensile strength model for full-size multifilament composites.

Tests were performed up to 400 or 850 °C for aluminium and titanium, respectively, in order to modify the stress transfer conditions along with the matrix properties. The above objectives are closely related to one another, especially for SiC–titanium whose use is anticipated for engine applications where both high temperatures and axial stresses are critical issues.

Other methods, like the push-out test, are currently applied in order to evaluate the extent to which the interface, i.e the fibre–protective coating–matrix interaction zone, has been effected by different processing and environmental conditions; these methods also provide information in terms of mechanical values. Moreover, push-out tests are relatively easy to perform on thin slices cut from plates, and the fibres submitted for testing are realistically surrounded by other fibres. Conversely, specially designed specimens containing only one filament are required for fragmentation.

Nevertheless, an interesting feature of the fragmentation test is that the tensile properties of the fibrous phase, that can be independently determined by testing the properly treated fibre in tension, is an integrated part of the fragmentation process together with the interface stress transfer capability. The fragmentation test actually is concerned with a tensile test on a model composite with many attributes being transferable to the actual unidirectional reinforced material, provided that the necessary adjustments have been made. This approach was illustrated a few years ago by Ochiai and Osamura [4], or Goda and Fukunaga [10], and forms the subject of Part II of this paper.

2. Materials and testing conditions

Three types of continuous SiC fibres have been used throughout the study, namely

1. Uncoated 100 μm diameter filament on 12 μm tungsten core (Sigma Composite Materials, a former German company; now available as SM 1040, from BP, UK).
2. A 140 μm diameter filament on 34 μm carbon core with a 3 μm carbon coating (SCS6, Textron, USA).

* *Present address*: SNECMA, Corbeil-Evry, France.
‡ To whom all correspondence should be addressed.

0022–2461

3. The same filament as in point 2; but with a 1.5 μm carbon coating (SCS2).

The first two fibres were associated with Ti–6Al–4V titanium alloy, and the last one with pure aluminium (1050 alloy) and aluminium–magnesium alloy (5083).

Monofilament model composites were prepared under the same conditions as the equivalent full-size composites. This point is very important with regard to the expected degradation of the fibre at processing temperatures. SiC–titanium monofilament tensile specimens were obtained by hot pressing a fibre between two 0.4 mm thick sheets of metal under vacuum, the fibre being kept in place during the first step of the consolidation by two spots from a fugitive binder (PMMA). Consolidation was made according to the superplastic forming–diffusion bonding (SPF–DB) process conditions of Ti–6Al–4V alloy, i.e. a pressure of 20–40 MPa was applied for 30 min at 925 °C. Samples of 0.6–0.7 mm thickness were first inspected by X-ray to check the fibre position and straightness; samples with a curved or broken fibre were discarded. Electric discharge machining gave flat dog-bone shaped specimens with a 35 mm gauge length and 4 mm width. The mean fibre volume fraction was 0.28% and 0.55% for materials with Sigma fibre and SCS6 fibre, respectively.

SiC–aluminium monofilament tensile specimens were obtained by carefully injecting the liquid alloy under inert gas into the mould containing the straight fibre. A temperature of 860 °C was maintained for 20 min. Flat sides were then machined on the gauge of the as-moulded 80 mm long 10 mm diameter cylinders to ensure good contact with the acoustic emission detector. Final specimens had a 32 mm gauge length of rectangular 4 × 2 mm cross-section. The mean fibre volume content was 0.18%.

Tensile tests were made at various temperatures with a crosshead speed of 0.5 mm min^{-1} (strain rate about 2.10^{-4} s^{-1}). At room temperature, progressive breaking of the SiC fibre was detected with acoustic emission (AE) by simply recording the number of events of high amplitude using a broad band Panametrics V105 transducer fitted with a CGR counter unit. At the same time, signals were detected with a second transducer, numerized via a transient recorder (Kontron) and sent to a microcomputer for analysis. The method has been reported elsewhere to be very reliable for fibre break monitoring and analysis [11]. According to the usual procedure, tests should be stopped when no new fibre break has been recorded for a long time with acoustic emission. In fact, there is a continuous yet decreasing AE throughout the test. Thus, tests were conducted until specimen necking or fracture occurred. Typical stress–strain curves are shown in Fig. 1 and will be discussed later. For high temperature tests, specimens were pre-heated for 20 min before a load was applied.

The specimens were observed after the mechanical test by optical and scanning electron microscopy. Preparation involved either surface polishing or partial dissolution of the metal matrix. The second method was preferred since the fragment's position is preserved, so relevant conclusions about the fibre–matrix modes of fracture can be made; this is a major issue in the interpretation of the fragmentation test data.

Single SiC fibres were also tensile tested in order to obtain strength distribution parameters of the different fibre batches, and to apply the proper scaling factor to derive the strength of short fibre fragments. As the relevant parameters are those of the *in situ* fibres and not the as-received ones, fibres were first given a treatment to put them into a state similar to that of the *in situ* fibres, thus taking into account possible degradation during processing. In the case of a titanium matrix, the treatment consisted of coating the fibres by ion sputtering with a ≈ 3 μm thick titanium layer, followed by a thermal cycle of 1 h at 925 °C. For aluminium, fibres were first infiltrated with the liquid metal according to the above processing conditions, then extracted by metal dissolution for tensile testing.

3. Fragmentation tests and results

Owing to the low fibre volume fraction and the high strain-to-failure of the matrix, SiC monofilament metal matrix composites undergo a multiple fracture process of the fibre during the tensile test. Increasing the load induces more and more breaks. The process stops when the stress transferred to the fragments at the interface is lower than the current fragment strength.

3.1. Multiple fracture process

Fig. 1 shows typical tensile curves and the associated acoustic emission (cumulated count number per second or count rate) at room temperature for specimens of the four materials, namely SCS2/1050, SCS2/5083, Sigma/Ti–6Al–4V and SCS6/Ti–6Al–4V. For both aluminium alloys, fibre fractures are detected both by a strong burst of AE and a drop in the load–displacement curve, but for the 1050 matrix only (Fig. 1a) counting of fractures is out of the question due to the poor yield strength of the alloy. For 5083 and the titanium matrices, there is some uncertainty as to what the exact number of fractures is, since AE shows many bursts:

1. With 5083 alloy, part of the acoustic emission is likely to come from plastic deformation of the metal, which also gives the small load drops that are easily observed on Fig. 1b. When analysed, the AE events of Fig. 1b correspond to either high energy or low energy events. They are plotted as a function of their time of occurrence in Fig. 2a, with some difficulty to rigorously identify their respective origin: the 11 upper points clearly correspond to fibre fractures, while the lower ones may be attributed either to secondary fibre fractures or to plastic deformation of the matrix. Observations that the signal amplitude decreases as the plastic deformation increases have been reported earlier [12].

2. With Ti–6Al–4V alloy, load drops are not visible but there is intense acoustic activity (Fig. 1c, d) especially with the Sigma fibre. AE starts in the elastic part

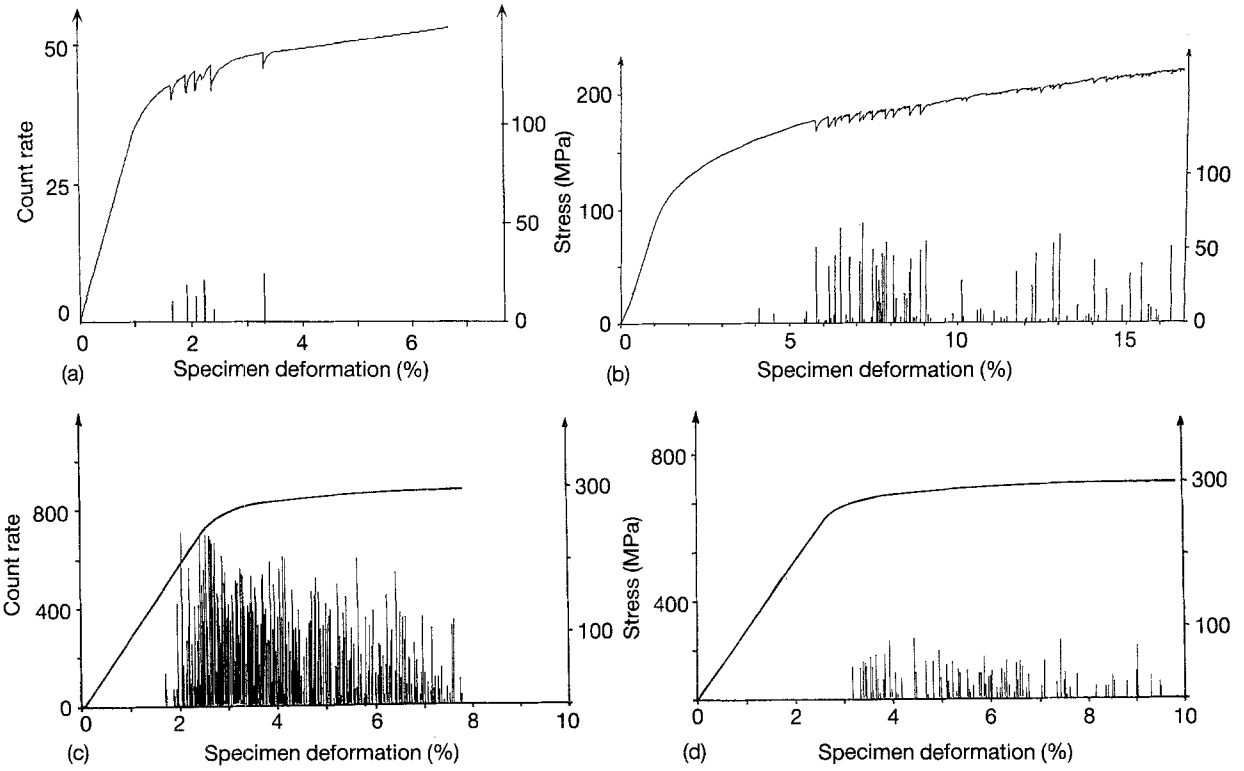

Figure 1 Typical room temperature fragmentation stress–strain curves and associated acoustic emission (count rate): (a) SCS2/1050, (b) SCS2/5083, (c) Sigma SiC/Ti–6Al–4V, and (d) SCS6/Ti–6Al–4V.

of the stress–strain curve for that fibre and at the yield point for SCS6. Again the signals, characterized by their energy content, are plotted on Fig. 2b where two groups are quite visible: the most energetic ones, with a decreasing energy content as the test proceeds, have been demonstrated to correspond to fibre fractures [11].

3.2. Fragment critical length

In the curves of Fig. 1, a steadily decreasing AE is recorded until the test is stopped, while signal analysis shows that most fibre fractures occur in the first per cent of strain. Now analysis of the fragmentation process is based on the final situation, "saturation", when the shorter and shorter fragments cannot be fractured under the stress resulting from shear reloading. As this final number of fragments must be known with high precision, the AE estimation has to be verified after partial removal of the matrix. For specimens tested at high temperature, only the final number of fragments could be determined.

In Fig. 3 are presented typical scanning electron microscope (SEM) photographs of the four materials (no fragmentation is observed in the tight ends of the stressed specimens): the main cracks, at distances several hundreds of microns apart, are the direct result of the fragmentation process, but they are accompanied, within a very short distance by a number of thin secondary cracks that originate in the shock wave produced by the main crack formation. For SCS6/Ti–6Al–4V (Fig. 3d), secondary cracks are often reduced to a branched main crack, giving the shape of a bevel-edged piece. Similar observations have been reported recently by Roman and Aharonov on

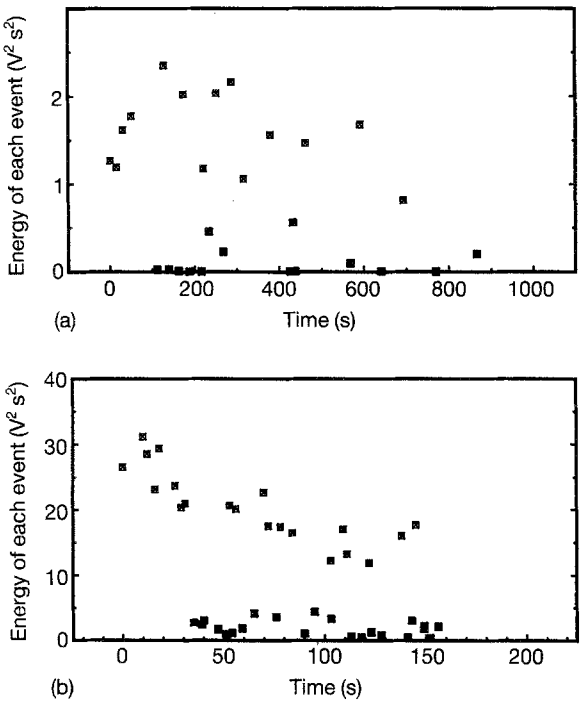

Figure 2 Energy analysis of acoustic emission signals: (a) SCS2/5083, and (b) SCS6/Ti–6Al–4V.

SiC–aluminium model composites [5]. Accounting was made for that multicracking when measuring the fragment length as the distance between two main cracks. Further conclusions from the SEM observations will be given in Section 4.2.

From the testing of several specimens, which gives a total of about 10–120 fragments for each system, mean fragment length, l_m, at room temperature is calculated and given in Table I for the four materials.

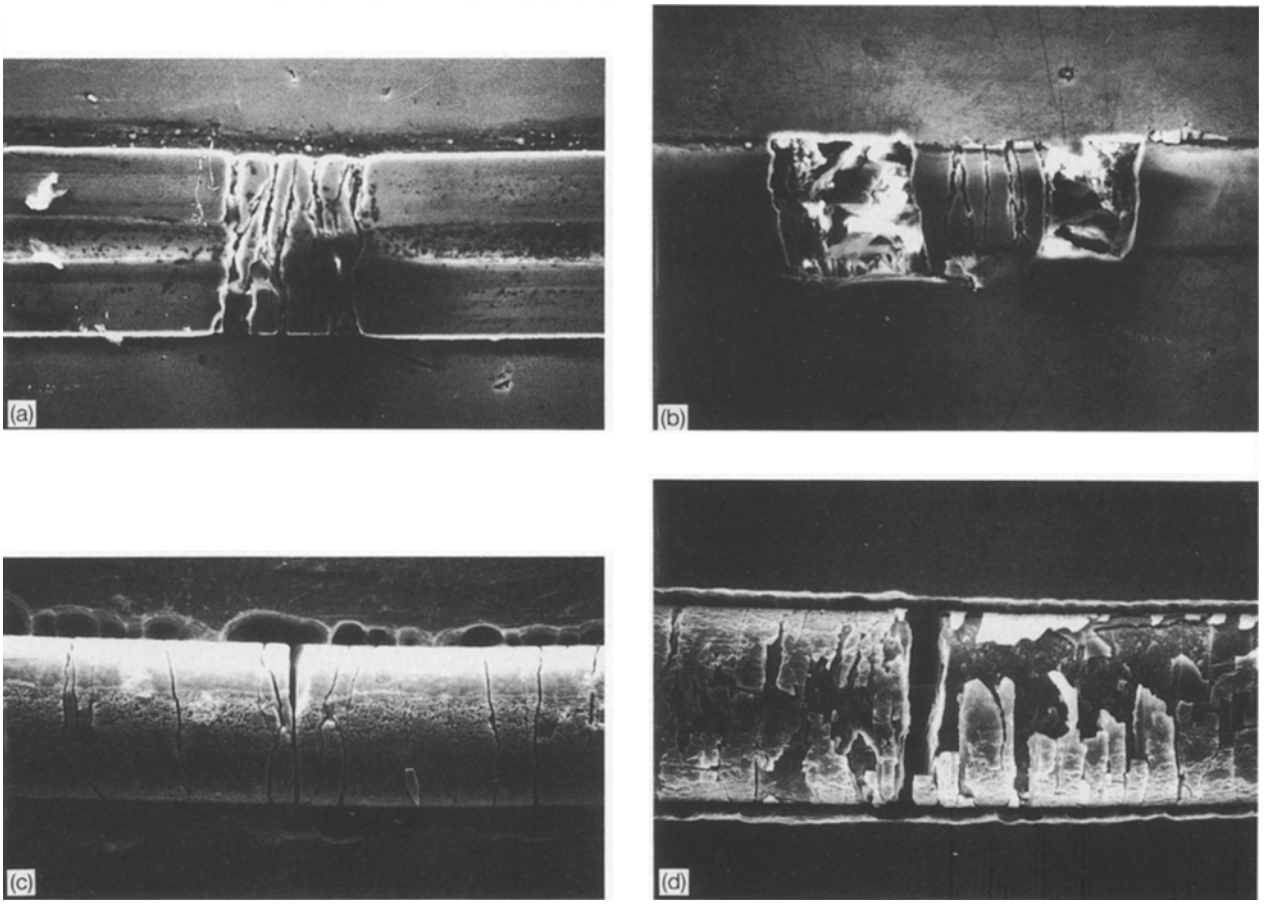

Figure 3 Typical main crack area of fragmented specimens (a, b) after polishing or (c, d) matrix dissolution. Fibre diameter: 140 μm (a, b, d) or 100 μm (c). (a) SCS2/1050, (b) SCS2/5083, (c) Sigma SiC/Ti–6Al–4V, and (d) SCS6/Ti–6Al–4V.

TABLE I Fragmentation test data

Material	l_m (μm)	l_c (μm)	CV1[a] (%)	CV2[b] (%)	l_c/d	τ_i (MPa)
SCS2/1050	3300	4400	44	5	32	46 ± 5
SCS2/5083	1410	1880	37	13	13	121 ± 10
Sigma/Ti–6Al–4V	266	355	65	8	3–4	350 ± 35
SCS6/Ti–6Al–4V	1147	1530	33	10	11	192 ± 20

[a] CV1, average of the coefficients of variation on l_c in reference to one specimen.
[b] CV2, coefficient of variation on the mean l_c for N specimens ($3 < N < 7$).
d is the fibre diameter and τ_i according to Equation 2.

Scatter is very high with the Sigma fibre (CV1 = 65%, with CV1 being an average, for the three specimens of this system, of the respective coefficient of variation on critical length, l_c) due to a lot of secondary cracks that preclude an exact estimation of what the mean length is. Specimen to specimen variation (CV2) is comparatively very low, which shows that the test reproducibility is good. According to previous work [13], the critical length, l_c, was roughly estimated as 4/3 of the mean length. This approximation ought to be re-examined in the light of recent models of the fragmentation test, where derivation of l_c from the observed length is not as deterministic as it is when using the simple 4/3 ratio.

The variation of l_c with temperature has been evaluated according to the same procedure for SCS6/Ti–6Al–4V up to 700 °C (Fig. 4). For the reasons given in Section 3.4., no fragmentation tests were made for the aluminium matrix specimens.

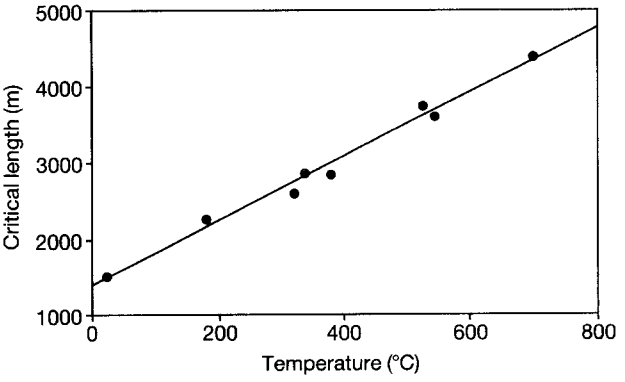

Figure 4 Critical length versus temperature (SCS6/Ti–6Al–4V).

3.3. Fibre strength at l_c

The strength-to-length relationship of each fibre has to be known in order both to calculate the interfacial shear stress and to be introduced into the simulation

that will be presented in Part II of this paper. As for the former, the fibre strength has to be determined at a length equivalent to l_c, which cannot be made directly by fibre testing. The common way is to test fibres at various lengths and extrapolate to l_c using Weibull gauging [13].

From observations of the fracture surfaces of broken filaments, it was assumed that, within the range of experimental lengths, internal flaws were responsible for the fracture. Accordingly, one can help using a bimodal distribution, which proved to be necessary when both surface and internal defects are present [14]. Now, the strentth distribution can be represented by a two parameter Weibull law, with the strength at any length, L_i, being given by

$$\ln \sigma_i = \ln \sigma_1 - \frac{1}{m} \ln L_i \quad (1)$$

where m and σ_1 are the shape parameters of the distribution and the strength of the filament of unit length, respectively. Strictly speaking, m ("average" Weibull modulus) ought to be the same as the one found by a statistical analysis of data at only one length ("local" modulus). In fact, whatever the length, the local modulus is always smaller than the average one, and data previously published on the basis of a determination of m from tests at one length [6] should be corrected accordingly. In addition, experimental determination of the fibre strength by the present method satisfies a basic requirement of the simulation presented in Part II where the strength-to-length relationship is a critical input.

A series of about 20 filaments was tested at various gauge lengths (in the range 5–60 mm) in their as-received state and after heat treatment aimed at reproducing the degradation of the fibres during processing. Results are given in Table II for 25 mm gauge lengths, together with the value of the Weibull modulus calculated from the slope of the ln strength – ln length relationship, using linear regression analysis (Fig. 5). To be noted is the difference between Sigma and SCS6 fibres: whereas there is a dramatic decrease in strength for the former, SCS6 appears to be more stable which is due to the presence of protective carbon coating (the tungsten core of the Sigma fibre may also react with silicon carbide during processing). The effect is also noticeable for SCS2, but in this case the temperature of the pretreatment (860 °C) was high enough to promote a heavy chemical reaction between SCS2 and the aluminium.

The strength of the fibres at l_c is obtained from Equation 1. A further assumption in the following is

TABLE II Tensile properties of SiC fibres

Fibre	As-received		Heat treated	
	σ_R[a] (MPa)	m	σ_R (MPa)	m
SCS2	3645	8.8	2335	7–8
Sigma	3430	6.3	725	6.7
SCS6	4195	17.0	3995	> 20.0

[a] σ_R given for 25 mm gauge length from the ln σ_R – ln length linear regression analysis.

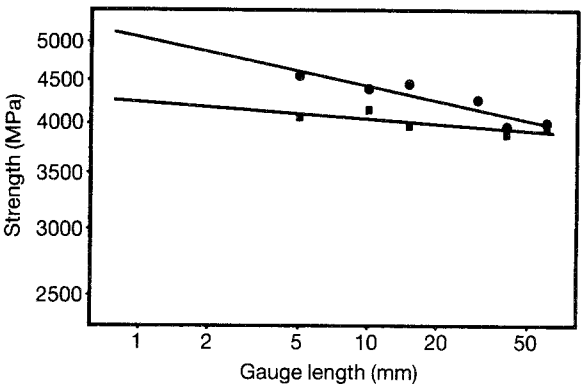

Figure 5 Strength-to-gauge length relationship for as-received (●) and heat-treated (■) SCS6 fibres with corresponding linear regression analysis. For as-received fibres, $\ln \sigma_R = \ln 5063 - \ln L/17.1$; correlation = 0.8847. For heat-treated fibres, $\ln \sigma_R = \ln 4288 - \ln L/45.4$; correlation = 0.8049.

that the Weibull modulus does not change with temperature which seems reasonable for short term exposures.

3.4. Interfacial shear strength

From the critical length and the corresponding fibre strength, the interfacial shear strength is calculated according to the familiar equation given by Kelly and Tyson [15] as

$$\tau_i = d\sigma_{R(l_c)}/2l_c \quad (2)$$

where d is the fibre diameter. It has been pointed out several times that Equation 2 covers a simplified representation of the interfacial stress state since, for a number of fibre–matrix systems, a mixture of elastic, frictional and plastic modes of stress transfer combine to give l_c. Without additional information about those modes, τ_i merely represents the overall ability for the interface to transfer stresses by shear.

Values of τ_i at room temperature are listed in Table I and the variation of τ_i versus temperature has been plotted in Fig. 6 for SCS6/Ti–6Al–4V. As expected from the increase in l_c in Fig. 4, a steady decrease in τ_i is calculated for this system. At any temperature, the interfacial shear strength is far lower than the shear stress, τ_y, of the Ti–6Al–4V alloy (560 MPa at room temperature), which means that modes other than plastic deformation of the matrix are involved in the interface failure. Room temperature values agree very well with the results reported by Le Petitcorps *et al.* [1] and Yang *et al.* [3].

Allowing a shear stress, τ_y, of about 45 and 120 MPa at room temperature for the 1050 and 5083 aluminium alloys, respectively, it seems obvious that plastic deformation is the limiting mode of stress building for those model composites. For the SCS2/6061 system, mean fragment lengths between 1.4 and 2.5 mm have also been reported by Hamann *et al.* [2]. It has thus been assumed that plastic deformation of the matrix is the limiting factor of the stress transfer for those systems, and that $\tau_i = \tau_y$ at any temperature. Fig. 6b, where the shear stress of the 6061 aluminium alloy, calculated from available tensile tests using Von Mises criterion, has been plotted

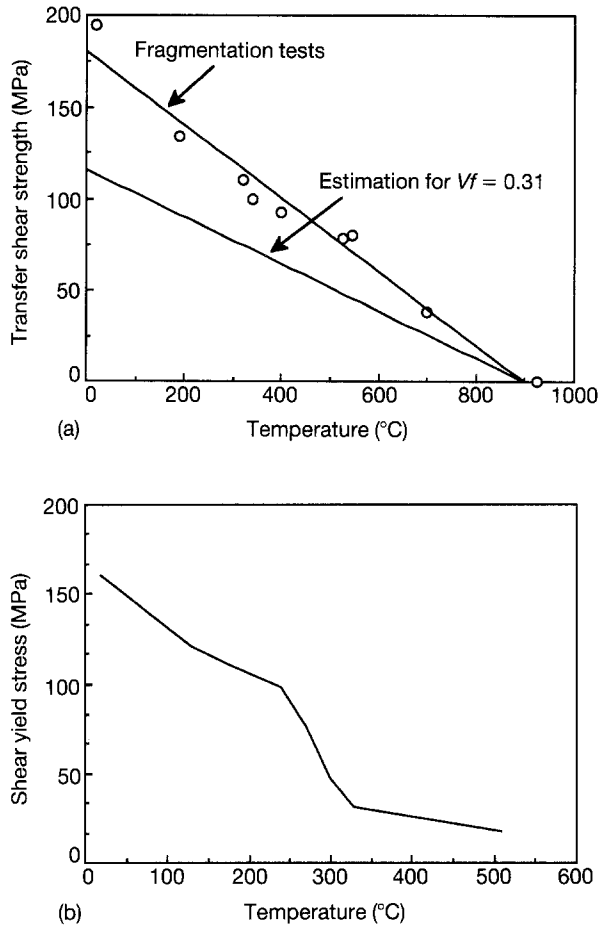

Figure 6 Transfer shear stress, τ_i, versus temperature: For (a) SCS6/Ti–6Al–4V, fragmentation test data and corrected τ_i for a 0.3 fibre volume fraction composite, and (b) SCS2/6061 (assuming $\tau_i \approx \tau_y$ of the metal alloy).

against temperature, gives the expected profile for τ_i. Higher values of the mean fragment length (5.1 and 2.9 mm, respectively) and corresponding smaller values of τ_i (41 and 71 MPa, respectively) have been reported by Roman and Aharonov [5] for SCS2/1100 and SCS2/6061 systems at room temperature. Based on these relatively low values of τ_i and their likeness with push-out test data, the authors come to other conclusions as regards the mode of stress transfer (see hereafter Section 4.2.).

4. Discussion

The fragmentation process has been well documented in the last few years. Notwithstanding the recent progress in the analysis and the comprehension of the fragmentation test (see for example references [13, 16]), the present paper does not incorporate the most recent models. Emphasis is, rather, put on the test ability to provide reasonable input values for a practical model of the tensile strength, incorporating a fibre–matrix stress transfer parameter.

4.1. Thermal stresses

The stress state in as-processed model composites was calculated at room temperature for a 0.25 fibre volume fraction by a finite element method, as well as by a conventional analytical method, using axisymmetric models with temperature dependent thermoelastic constants. Results of both methods match quite well and are given in Table III for the temperature tested systems (z, direction along fibre axis, r and θ radial and tangential directions, respectively). In the aluminium matrix, SCS2 is under axial and radial compression, while tangential stress is positive near the fibre surface (0.2 mm) but negative at the interface. Higher stresses are predicted for SCS6 in titanium.

The σ_{zz} value was experimentally confirmed (= $E\delta_{zz}$ with E, Young's modulus) from the overlapping length of the broken fibre ends, after partial dissolution of the matrix (Experiment 1 in Table III), or from the strain at which the first high-amplitude event was recorded (Experiment 2) in the tensile test using

$$\varepsilon_{zz} = \varepsilon_{fR} - \varepsilon_c \quad (3)$$

where ε_{fR} is the average rupture strain of a fibre of length equal to the specimen gauge length (from properties of heat-treated fibres in Table II) and ε_c the specimen strain at the first AE event. With SCS6, σ_{zz} was found to be about zero, which is a result of the strong plastic flow of the titanium alloy in the fibre direction during pressing at high temperature putting the SiC fibre in tension first, which is entirely counterbalanced by the thermal mismatch effect upon cooling down. The radial stress was not assumed to be affected by the plastic flow.

According to the above values for σ_{zz}, the *in situ* ultimate strain, ε_c, of the fibre was compared to the specimen strain at the first AE event. Agreement is quite acceptable except for the Sigma/Ti–6Al–4V system where the expected 0.18% value is far from the experimental one (Table IV). The difference is likely to be attributed to an excessive degradation of the fibre during the treatment preceding the fibre strength determination.

TABLE III Thermal stresses at room temperature (in MPa) in monofilament composites

	σ_{zz}			σ_{rr}	$\sigma_{\theta\theta}$
	Calc.	Exp. 1[a]	Exp. 2[b]	Calc.	Calc.
SiC/5083[c]	− 5000	− 5000	− 4400	− 250	+ 75
SiC/Ti–6Al–4V[c]	− 1700	≥ 0	≈ 0	− 360	+ 360

[a] Experiment 1 is from the overlapping fibre ends.
[b] Experiment 2 is from the acoustic emission CTE input values at room temperature.
[c] Fibres = $5.10^{-6}\,°C^{-1}$, isotropic; 5083 alloy = $25.10^{-6}\,°C^{-1}$; Ti–6Al–4V = $10.10^{-6}\,°C^{-1}$.

TABLE IV Comparison of calculated (according to Equation 3) and observed strains at first fibre fracture (%)

	ε_{fR}[a]	ε_{zz}	ε_c	
			Calculated	Experimental
SCS2–Aluminium	0.60	1.25	1.85	1.90–2.50
Sigma–Titanium	0.18	0.00	0.18	0.60
SCS6–Titanium	1.10	0.00	1.10	1.20

[a] ε_{fR} is the fibre ultimate strain at specimen gauge length.

4.2. Signifying τ_i

With the present systems, fibre fracture occurs mainly after matrix yield stress; but locally, near the broken fibre ends, plastic deformation may be very high compared to the overall plastic deformation. From SEM observations on a 3% strained SCS2/5083 specimen, local strains as high as 17% have been measured with shear bands extending in the matrix at 45° to the fibre surface. This is a justification for using Equation 2 to calculate τ_i since the Kelly–Tyson model specifically applies to systems where stress transfer involves the plastic deformation of the matrix. In the present case, this plastic deformation occurs along the carbon coating that protects the fibre surface. As that coating is quite brittle in comparison with the SiC fibre, it is affected by multiple fracture as suggested by Le Petitcorps [17]: in tests which were stopped just beyond the macroscopic yield point, a severely degraded coating is readily observed close to the fibre broken ends, while the fibre itself is broken only at a few points.

The quantity τ_i is thus the overall result of stress being transferred both by plastic deformation at the matrix–coating interface and by friction at the coating–fibre interface. With an aluminium matrix, transfer is apparently limited by the matrix shear properties, while a mixture of friction and plastic deformation operates with titanium. It has to be pointed out that those conclusions strictly apply to the monofilament model composites: with higher volume fractions (unidirectional composites), where the fibres become very close to each other, other conditions are met according to the actual stress state around the fibres. In addition, temperature may also effect the stress state.

4.3. Temperature dependence of τ_i

According to previous work [13], when debonding occurs at the fibre–matrix interface in the fragmentation test, the transfer shear stress can be written as a function f as

$$\tau_i = f(\tau_d, \tau_f) \quad (4)$$

where τ_d is the debonding strength and τ_f the frictional stress depending on the actual stress state at the interface according to $\tau_f = \mu\sigma_{RR}$ (Poisson's and thermal effects with μ a coefficient of friction and σ_{RR} radial stress). With the current metal matrix, Equation 4 changes to Equation 5

$$\tau_i = f(\tau_d, \tau_f, \tau_y) \quad (5)$$

As reported recently by Cheneau and Auvray for carbon–BMI systems, τ_d, when directly measured by a pull-out test, shows some temperature dependence, a part of it being due to the thermal stresses progressively relaxing in the test support which influences the measured pull-out stress [18]. For the sake of simplicity, τ_d will be assumed to be constant, and only τ_f and τ_y will be temperature dependent. Two extreme cases may occur

1. If $\tau_d < \tau_y$ but $\tau_f \gg \tau_y$, or $\tau_d > \tau_y$, within the whole temperature range, matrix yielding and plastic flow take place after (or without) first debonding. Stress transfer is thus controlled by τ_y, and $\tau_i(T)$ approximately reflects $\tau_y(T)$ of the metal alloy (disregarding the matrix strain-hardening coming from the metal constraint close to the fibre surface). This is the case of the SiC–aluminium composites. It has been pointed out in Section 3.2 that another explanation for the SiC–aluminium fragmentation tests has been put forward by Roman and Aharonov [5]: observing that the debonding strength calculated from both fragmentation and push-out tests is comparable to the friction stress obtained when SCS2 fibres are pushed back through the matrix (71, 60 and 57 MPa, respectively), they conclude that the stress transfer in SCS2/6061 is attributed mainly to friction, with no consideration being given to the matrix properties (whose shear strength is 83 MPa).

2. If $\tau_f \ll \tau_y$ and $\tau_d \ll \tau_y$ within the whole temperature range, friction follows after debonding, long before matrix yielding. Stress transfer is now controlled by interfacial friction with $\tau_i(T)$ reproducing the $\tau_f(T)$ variation or the $\sigma_{RR}(T)$ variation if the coefficient of friction remains unchanged. This is the case of SiC–titanium composites.

4.4. Extension to unidirectional composites

Extending the above statements to unidirectional composites is straightforward, as long as it is accepted that fibre-to-fibre stress transfer mechanisms in multifilament materials are similar to those active in the model composites studied so far. For aluminium-based materials, it is proposed that stress transfer will be mainly controlled by the matrix properties in the shape of $\tau_i(T)$ of Fig. 6b, with some possible contribution from matrix strain-hardening due to a triaxial stress state in the presence of surrounding fibres.

As far as titanium-based materials are concerned, the fibre volume fraction cannot be overlooked because it has a direct effect on the radial stress that controls τ_i and thus the fibre-to-fibre transfer stress. As regards σ_{RR}, Sun *et al.*, referring to a simple strength of materials approach for a square array of SCS6 fibres in a Ti–6Al–4V matrix, reported a compressive value of 107 MPa for a composite of 0.4 fibre volume fraction with slightly different material constants [19]. Computing the thermal stresses, corresponding to a composite with $Vf = 0.3$, by the aforementioned finite element program gives a radial compression of 260 MPa, instead of 360 MPa in the case of a monofilament composite at room temperature.

Assuming, as noted previously, that $\tau_i \propto \tau_f$ or $\tau_i \propto \mu\sigma_{RR}$, with μ constant, and $\tau_i = 0$ at the processing temperature, a corrected value τ_i^* can be derived that obviously changes as τ_i does (cf., Fig. 6a) when temperature increases. τ_i^* is the effective transfer stress for a 0.3 volume fraction SiC–titanium unidirectional composite, and will be used as the interface contribution. It has to be noted that stresses are of the same sign whatever the volume fraction, which means that a single mode of stress transfer operates at any temperature.

5. Conclusions

Fibre–matrix transfer stress has been measured by fragmentation tests on four SiC–aluminium and SiC–titanium monofilament model composites at room temperature. For SCS6/Ti–6Al–4V, tests have also been performed at various temperatures. Mechanisms of load transfer have been identified to be mainly controlled by matrix mechanical properties for SCS2/5083 and by post-debonding friction arising from radial compression around the fibre for SCS6/Ti–6Al–4V.

Based on the hypothesis that similar mechanisms are involved in unidirectional composites of practical volume fraction, it is suggested that the transfer shear stress can be used as an input parameter accounting for the interface contribution in a model of tensile fracture of multifilament unidirectional composites. This will form Part II of this paper.

References

1. Y. LE PETITCORPS, R. PAILLER and R. NASLAIN, *Comp. Sci. Technol.* **35** (1989) 207.
2. R. HAMANN, J. CHICOIS, P. FLEISCHMANN, R. FOUGÈRES and P-F. GOBIN, in "Fourth European Conference Composite Materials (ECCM-4)", edited by J. Füller, G. Grüninger, K. Schulte, A. R. Bunsell and A. Massiah (Elsevier, London, 1990) pp. 375–380.
3. J-M. YANG, S. M. JENG and C. J. YANG, *Mater. Sci. Engng* **A138** (1991) 155.
4. S. OCHIAI and K. OSAMURA, *J. Mater. Sci.* **23** (1988) 886.
5. I. ROMAN and R. AHARONOV, *Acta Metall. Mater.* **40** (1992) 477.
6. A. VASSEL, M-C. MÉRIENNE, F. PAUTONNIER, L. MOLLIEX and J-P. FAVRE, in "Sixth World Conference on Titanium", (Les Editions de Physique, Paris, 1989) pp. 919–923.
7. L. MOLLIEX, J-P. FAVRE and A. VASSEL, in "1990 International Conference on Titanium Production and Application", Vol. 1, (TDA, Dayton, 1990) pp. 180–188.
8. L. MOLLIEX and J-P. FAVRE, in "Septiémes Journées Nationales sur les Composites (JNC-7)", edited by G. Fantozzi and P. Fleischmann (AMAC, Paris, 1990) pp. 207–215.
9. L. MOLLIEX, J-P. FAVRE and A. VASSEL, in "Interfacial Phenomena in Composite Materials (IPCM'91)", edited by I. Verpoest and F. Jones (Butterworth-Heinemann, Oxford, 1991) pp. 183–186.
10. K. GODA and H. FUKUNAGA, *Comp. Sci. Technol.* **35** (1989) 181.
11. M-C. MÉRIENNE and J-P. FAVRE, in "Third International Symposium on Acoustic Emission from Composite Materials (AECM-3)", (ASNT, Inc., Columbus, 1989) pp. 304–312.
12. H. L. DUNEGAN and A. T. GREEN, ASTM STP 505 (ASTM, Philadelphia, 1972) pp. 100–113.
13. J-P. FAVRE and D. JACQUES, *J. Mater. Sci.* **25** (1990) 1373.
14. K. GODA and H. FUKUNAGA, *ibid.* **21** (1986) 4475.
15. A. KELLY and W. R. TYSON, *J. Mech. Phys. Solids* **13** (1965) 329.
16. P. FEILLARD, G. DÉSARMOT and J-P. FAVRE, *Comp. Sci. Technol.* **49** (1993) 109.
17. Y. LE PETITCORPS, Thèse Université de Bordeaux (1985).
18. P. CHENEAU and M-H. AUVRAY, in "Huitiémes Journées Nationales sur les Composites (JNC-8)", edited by O. Allix, J-P. Favre and P. Ladevèze (AMAC, Paris, 1992) pp. 301–311.
19. C. T. SUN, J. L. CHEN, G. T. SHA and W. E. KOOP, *J. Compos. Mater.* **24** (1990) 1029.

Received 21 January 1993
and accepted 21 March 1994